CHAPTER 5

Modified Ripple Correlation Control MPPT with Single-phase Single-stage Two Cascaded H-bridge Multilevel VSI for Grid-connected Photovoltaic Systems

5.1 Introduction and outline

Grid connected photovoltaic (PV) systems have had an enormous increase in their market share over the last decade [1]. However the efficiency of commercial PV panels is around 15-25%. Therefore, it is very important that the power produced by these panels is not wasted, by using an efficient grid-connected inverter. Grid-connected inverter technologies for PV systems consist of 4 types: 1) centralized, 2) string, 3) multi-string, and 4) AC-module technology. The string technology is mostly used commercially and is more efficient than the centralized but it cannot solve the mismatch losses and high voltage stress in power switches. The multi-string technology is developed by adding many strings, each interfaced with its own dc/dc converter, each string can be independently controlled to operate at the maximum power point (MPP) of the string, and is very flexible. However the multi-string has two states of power processing that cause more power losses in power switches, and copper losses in dc wires due to connecting many PV strings [8]. The transformerless cascaded H-bridge multi-level voltage source inverter (CHB-MLI) merges the benefits of string and multi-string technology. It combines the improved maximum power point tracking (MPPT) independently for many strings connected in a series and operating as a single-stage power processing inverter. There are numerous advantages of using the CHB-MLI for grid-connected PV systems, such as low THD, small filter size, high efficiency, low stress voltage of power switches, and reduced losses from mismatch effect and partial shading. Additionally the CHB-MLI has many H-bridge cells series-connected, each H-bridge cell needs isolated dc-power sources, which can be easily supplied by PV

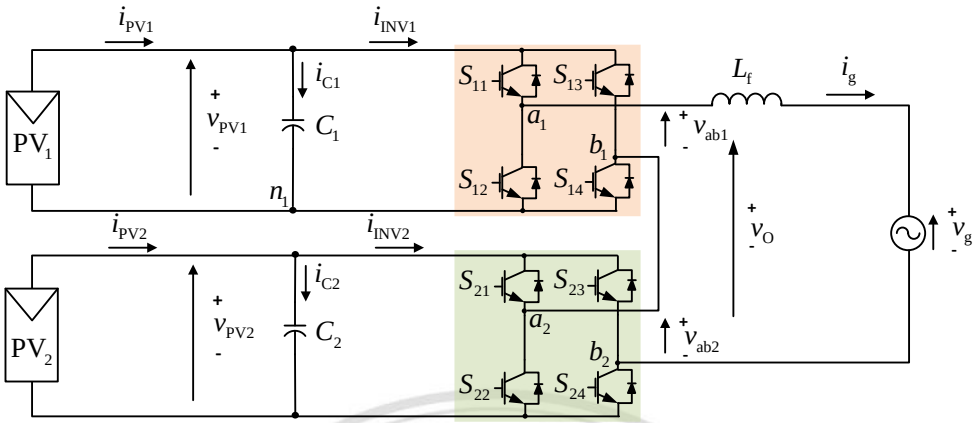

Figure 5.1 The power scheme of single-phase single-stage CHB-MLI for GCPVS.

modules or strings. From these features, the CHB-MLI topology is suitable for grid-connected PV systems (GCPVS) [10],[18].

The CHB-MLI topology is designed for supporting the independent MPPT for each H-bridge cell. Furthermore, the characteristic of PV power is nonlinear and time varying caused by changing the atmospheric conditions [31]. Using the suitable MPPT algorithm can increase the efficiency of MPPT and GCPVS. Numerous MPPT techniques have been proposed such as hill-climbing, fractional open-circuit voltage control, P&O, incremental conductance (INC), fractional short-circuit current control, fuzzy logic control, neural network, ripple-correlation control and several others [27]. The ripple-correlation control MPPT (RCC-MPPT) is the one which is convenient for GCPVS with the following features: very fast convergence to reach MPP, parameter-insensitive MPPT of PV systems, several straightforward circuit implementations and well developed theoretical basis. It would be suitable for a modular application, which uses small converters and the applications requiring a high rate of convergence [28]-[29]. However, the conventional RCC-MPPT has some disadvantages relating to the definition of suitable time constants of the filters to generate the desired output signal for correct MPPT control. It slows down reaching the MPP of PV operating, especially in the case of rapid shading irradiance. In this paper, to overcome that disadvantage, the RCC-MPPT has been modified using the mean function concept to generate the corrected ripple signal and make the MPP operating more accurate. In the ac-side of GCPVS, to ensure that grid-connected inverters have to inject the sinusoidal current into the utility grid, according to the specific standards defined by the utility in each country.

The control technique for injecting power to the grid in this paper is developed using the current control, based on the principle of rotating reference frame for the proposed single-phase CHB-MLI scheme. This emphasized that the injecting active and reactive power can be controlled separately.

This thesis proposed the control method of CHB-MLI for GCPVS by using the modified RCC-MPPT method to guarantee the accurate MPP operating of power transfer from each PV string, and fast MPPT strings in case of rapidly changing of irradiation, and using the current control based on the rotating reference frame theory for injecting the active and reactive power to the utility grid.

5.2 Modeling and analysis of the proposed modified RCC-MPPT with the single-phase single-stage two cascaded H-bridge multilevel VSI for grid-connected photovoltaic systems

Figure.1 shows the power scheme configuration of the single-phase single-stage CHB-MLI grid-connected PV system consisting of two H-bridge power cells which are series-connected their output terminals. Each H-bridge cell has its own PV string power supply parallel-connected with the decoupling capacitor. The output terminals of CHB-MLI are connected to the grid through the inductive filter to reduce the derivative and harmonic distortion of the grid current. The output voltage of CHB-MLI is synthesized by summing the two cascaded H-bridge inverter output voltages. It can generate between three and nine voltage levels depending on the selected control technique, It can be given by

$$v_o = \sum_{m=1}^{n} (S_{m1} - S_{m3}).v_{\mathrm{PV}m} \ , \ S_{m1}, S_{m3} \in \{0,1\} \tag{5.1}$$

where m and n are the order number and the number of cascaded H-bridge units in the PV systems, respectively. The relationships of instantaneous PV power between grid power, instantaneous capacitor power, and instantaneous inductor power, in case of unity power factor and neglecting power losses in CHB-MLI, is given by

$$p_{\mathrm{PV}} = p_{\mathrm{C}} + p_{\mathrm{L}} + P_{\mathrm{grid}}(1 - \cos\ (2\omega t)) \tag{5.2}$$

where p_{PV} is the instantaneous PV power.

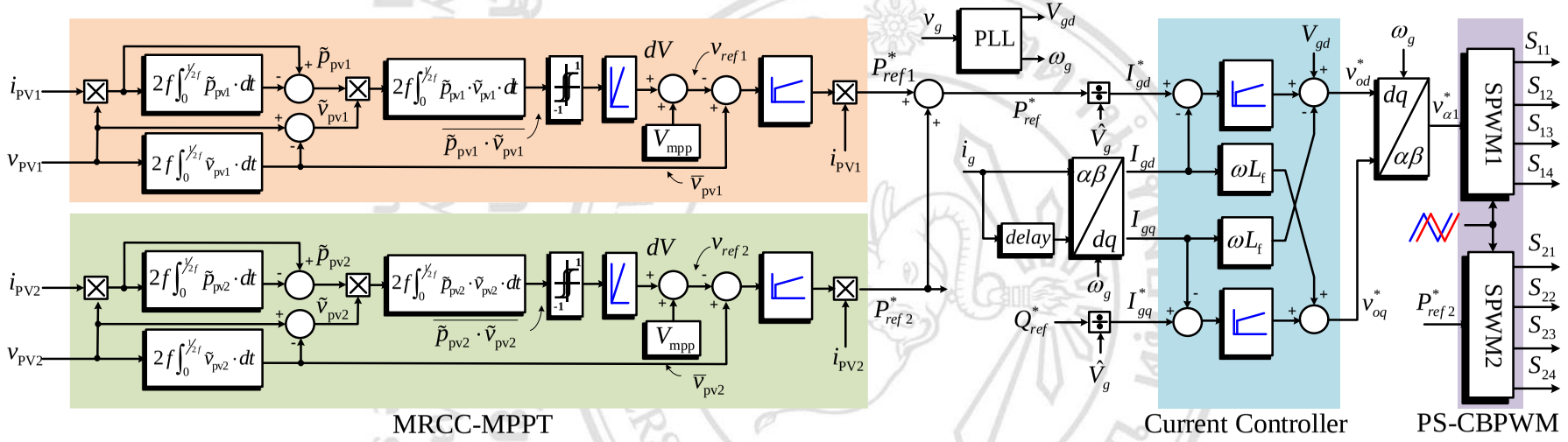

Figure 5.2 Proposed MRCC-MPPT, current control and modulation control techniques for two H-bridge cells CHB-MLI for GCPVS

Figure 5.2 shows the proposed control scheme for two H-bridge cells CHB-MLI consisting of three main parts; the modulation control technique, the MRCC-MPPT technique and the current control technique. The information of the proposed control technique can be detailed as follow.

5.2.1 Modulation control

From the Figurer 5.2, the power switches are controlled with the unipolar and phase-shifted carrier-based pulse width modulation (PS-CBPWM) techniques. In this section, the control of two cascaded H-bridge inverters based on the PS-CBPWM control technique is analyzed.

Figure 5.3 shows the operating diagram of the PS-CBPWM strategy to generate eight gate signals for the two cascading H-bridge inverters. This technique is applied from the simple unipolar phase-shifted modulation, where v_{mod} is the two sinusoidal modulating waves, which have the same magnitude and frequency but are 180º out of phase. The sign of subtraction between the reference waves and the carrier waves is converted to produce gate signals with the condition to produce "1" when the sign is "+" and "0" when the sign is "-". It is sent to generate two gate signals to control two switches of each leg, in the H-bridge unit, with opposite state. This technique can generate the high frequency in each voltage level of output voltage, it is double the carrier frequency and multiplied by the number of cascaded H-bridge, and given by

$$f_o = 2 \cdot H \cdot f_{cr} . \tag{5.3}$$

In addition, the v_{cr} and $v_{\text{cr+90}}$ is the two triangular waves, which are shifted with the phase-shifted angle φ, given by

$$\varphi = \frac{(q-1)\pi}{H} \tag{5.4}$$

where H and q are the number and the order number of H-bridge cells.

Form (5.2), in this case, is the principle of phase-shifted modulation for a two cascading H-bridge inverter, where two triangular carriers are required with a $90°$ phase displacement between any two adjacent carriers, $\varphi_1 = 0°$ for upper H-bridge $(q = 1)$ and $\varphi_2 = 90°$ for lower H-bridge $(q = 2)$ (Figure 5.4). In case of the PV input voltage of both H-bridges are equal, the waveform of output voltage can be produced in five voltage levels, for which the operating principle is shown in Figure 5.4.

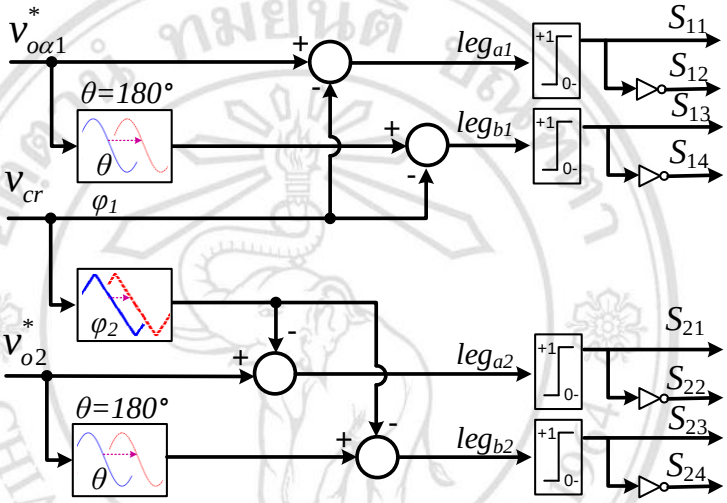

Figure 5.3 Modulation scheme for two single-phase cascaded H-bridge inverters with PS-CBPWM strategy.

The key waveforms of this strategy are shown in Figure 5.4, the inverter operating under the condition of the fundamental frequency $f_1 = 50$ Hz, the frequency modulation index $m_f = 7$, and the amplitude modulation index $m_a = 0.9$. The two modulation waves are compared with the two common phase-shifted triangular carrier waves, generating four inverter pole voltages, $v_{an1}, v_{bn1}, v_{an2}$, and v_{bn2}, respectively. All waveforms of the inverter pole voltages can be derived, from which the inverter terminal output voltages can be found from $v_{ab1} = v_{an1} - v_{bn1}$ and $v_{ab2} = v_{an2} - v_{bn2}$.

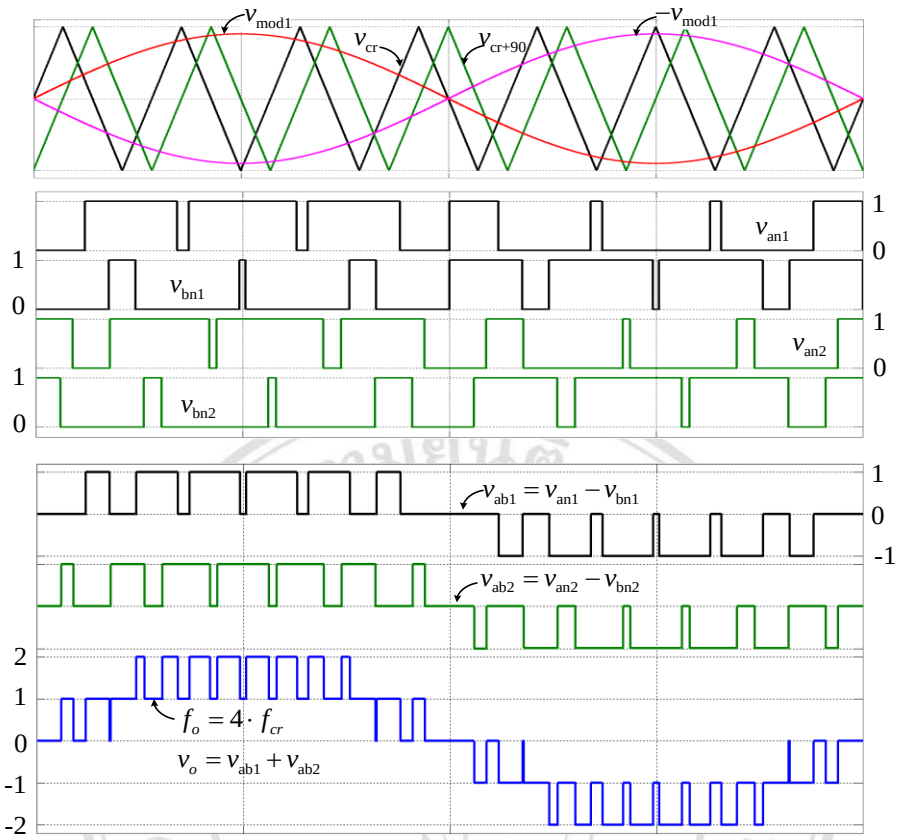

Figure.5.4. Phase-shifted carrier-based PWM for a 2-H-bridge CHB-MLI with amplitude modulation ratio $m_a = 0.9$ and frequency modulation ratio $m_f = 7$.

Finally, the waveform of two cascaded H-bridge inverters output voltage v_o is composed of five voltage levels with a peak value of *2E*, can be found from $v_o = v_{ab1} + v_{ab2}$.

5.2.2 Modified RCC-MPPT

The most of MPPT algorithms are based on the tracking of the maximum power operating point, which is the minimum derivative or partial derivative of the change in PV output power ∂p at the change in PV voltage ∂v, it can be written as $\partial p / \partial v = 0$. The value of power derivative $\partial p / \partial v$ is an important variable to define the reference PV voltage v_{ref} in the dc-link voltage controller for reaching the MPP.

Figure 5.5 shows the three curves of PV characteristic, *i*-*v* curve, *p*-*v* curve and power derivative $\partial p / \partial v$ curve, where MPP is the top of *p*-*v* curve and the power derivative $\partial p / \partial v = 0$. The MPPT algorithms force the PV systems to track the MPP by regulating the PV voltage v_{PV}.The RCC-MPPT method uses the instantaneous PV power ripple $\tilde{p}_{\mathrm{PV}}$ and the instantaneous PV voltage ripple $\tilde{v}_{\mathrm{PV}}$, which are the inherent alternative components in single-phase GCPVS, to find out the power derivative $\partial p / \partial v$.This method needs to know the oscillation frequency f_{os} which is double the grid frequency f_1, $f_{os} = 2f$ to correct the MPPT algorithm operating. The mean function concept is used for finding instantaneous PV voltage ripple and instantaneous PV power ripple as

$$\tilde{v}_{\mathrm{PV}} = v_{\mathrm{PV}} - \overline{v}_{\mathrm{PV}}, \tag{5.5}$$

$$\tilde{p}_{\mathrm{PV}} = p_{\mathrm{PV}} - \overline{p}_{\mathrm{PV}}, \tag{5.6}$$

where $\overline{v}_{\mathrm{PV}}$ and $\overline{p}_{\mathrm{PV}}$ are the DC components of PV voltage and PV power, respectively.

The power derivative $\partial p / \partial v$ is given by

$$\frac{\partial p}{\partial v} \cong \frac{2f \int_{t-1/2f}^{t} \tilde{p}_{\mathrm{PV}} \cdot \tilde{v}_{\mathrm{PV}} \cdot dt}{2f \int_{t-1/2f}^{t} \tilde{v}_{\mathrm{PV}} \cdot \tilde{v}_{\mathrm{PV}} \cdot dt} \cong \frac{\overline{\tilde{p}_{\mathrm{PV}} \cdot \tilde{v}_{\mathrm{PV}}}}{\overline{\tilde{v}_{\mathrm{PV}} \cdot \tilde{v}_{\mathrm{PV}}}}. \tag{5.7}$$

This research proposes the modified RCC-MPPT (MRCC-MPPT) by using the moving average or mean function as the main process in order to overcome the complicacy to define the suitable time constant of using the 1st order HPFs and 1st order LPFs in the conventional technique [29]. It also generates a fast response for the desired output signal in case of rapidly shading irradiance.

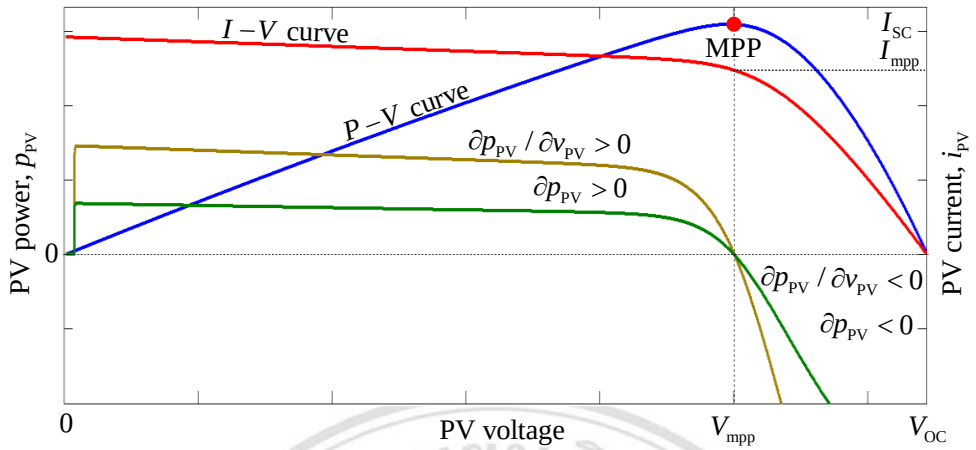

Figure 5.5 The typical *p-v*, *i-v* curves and the simulation result of power derivative $\partial p / \partial v$ and the change of PV power ∂p of a PV string.

From the simulation results in Figure 5.5, the curve of power derivative $\partial p / \partial v$ and the curve of the upper term of power derivative $\partial p = \overline{\tilde{p}_{PV} . \tilde{v}_{PV}}$ can be met at the zero point at the same PV voltage, at the MPP. It indicates that the curve of ∂p can be used to find the MPP correctly as the curve of power derivative $\partial p / \partial v$.

The block diagram of the proposed MRCC-MPPT and dc-link voltage controller are shown in Figure 5.2. In this case, it has two sets of MRCC-MPPT dc-link voltage controllers for two H-bridge cells, which have the same operation. For example of H-bridge1, the MRCC-MPPT only uses the mean function to find out the mean term of instantaneous PV power $\overline{p}_{PV1}$ and mean term of instantaneous PV voltage $\overline{v}_{PV1}$. They are subtracted from the instantaneous PV power p_{PV1} and instantaneous PV voltage v_{PV1} to keep their ripples and multiply them to get the product ripple $\tilde{p}_{PV1} \cdot \tilde{v}_{PV1}$. The mean function is used again to find the output of $\partial p = \overline{\tilde{p}_{PV1} \cdot \tilde{v}_{PV1}}$.

This method still uses the sign function to generate +1 if the $\overline{\tilde{p}_{PV1} \cdot \tilde{v}_{PV1}} > 0$ or -1 if the $\overline{\tilde{p}_{PV1} \cdot \tilde{v}_{PV1}} < 0$, which is converted to be an element of the reference voltage v^*_{ref1} through the integrate function block. To

control the dc-link voltage through the difference between the mean of feedback PV voltage $\overline{v}_{\mathrm{PV1}}$, the reference voltage v_{ref1} and the PI controller, the reference active power p^{*}_{ref1} can be produced as it is simply a product of output of dc-link voltage controller and PV current i_{PV1}. It causes the output of each dc-link voltage controller to produce a reference active power for each PV string. The reference active power of PV_2 p^{*}_{ref2} is used to control the power switches in H-bridge2 directly in order to maximize power from PV_2 to the utility grid.

5.2.3 Active and reactive powers controller

In order to control the injecting active power and reactive power to the utility grid independently for GCPVS, this paper uses the current control technique based-on the principle of rotating reference frame to be the controller model of proposed GCPVS as shown in Figure 5.2. The single-phase voltage equation in the ac-side of the proposed GCPVS can be written in $\alpha\beta$ stationary reference frame as

$$\begin{bmatrix} v_{o\alpha} \\ v_{o\beta} \end{bmatrix} = L_{\mathrm{f}} \frac{d}{dt} \begin{bmatrix} i_{g\alpha} \\ i_{g\beta} \end{bmatrix} + \begin{bmatrix} V_{g\alpha} \\ V_{g\beta} \end{bmatrix} \tag{5.8}$$

where $v_{o\alpha}, v_{o\beta}$ are the output voltage of CHB-MLI, $V_{g\alpha}, V_{g\beta}$ are the grid voltage, and $i_{g\alpha}, i_{g\beta}$ are grid current.

In the rotating reference frame, the active power and the reactive power are given by

$$\begin{aligned} p &= \frac{1}{2} V_{\mathrm{gd}} \cdot i_{\mathrm{gd}} \\ q &= \frac{1}{2} V_{\mathrm{gd}} \cdot i_{\mathrm{gq}} \end{aligned} \tag{5.9}$$

where V_{gd}, V_{gq} are the grid voltages , and i_{gd}, i_{gq} are the grid currents in dq rotating reference frame.

In Figure 5.2, there are two current feedback control loops in the current control scheme for the accurate control of grid currents i_{gd} and i_{gq}.To generate the proper grid voltage orientation, the voltage and current in (5.8) have to be transformed to the two-phase voltage and current in *dq* rotating reference frame in order to generate the desired active and reactive power components. The reference output voltages of CHB-MLI v_{gd}^{*}, v_{gd}^{*} produced by the controller are given by

$$\begin{bmatrix} v_{od}^{*} \\ v_{oq}^{*} \end{bmatrix} = L_{\mathrm{f}} \frac{d}{dt} \begin{bmatrix} i_{gd}^{*} \\ i_{gd}^{*} \end{bmatrix} + \omega_g . L_{\mathrm{f}} \begin{bmatrix} -i_{gd}^{*} \\ i_{gd}^{*} \end{bmatrix} + \begin{bmatrix} V_{gd} \\ V_{gq} \end{bmatrix} \tag{5.10}$$

The modulation control signal of H-brigde1 is the reference output voltage $v_{o\alpha}^{*}$, which can be generated by transforming the output voltages reference of CHB-MLI v_{od}^{*}, v_{oq}^{*} in the *dq* rotating reference frame to be the reference output voltages of CHB-MLI in $\alpha\beta$ stationary reference frame.

5.3 Simulation results

The PV system structure and control scheme shown in Figure 5.1 and Figure 5.2 have been implemented in MATLAB/SIMULINK in order to verify the behavior of the proposed control scheme. The model of the PV module is the single-diode model, the characteristic of the cells and equations are implemented according to [33]. The two sets of 8 PV panels supplied to each H-bridge in the CHB-MLI. The parameters of each PV panel and the parameters of the PV system are shown in Table 5.1. To substantiate the operating of the control system, the investigation is designed to regard the following points: 1) to track MPP with rapidly changing irradiance to testify the authentic precision and convergence speed of the proposed MRCC-MPPT technique for the single-stage single-phase CHB-MLI GCPVS, 2) to control active and reactive power for the single-stage single-phase CHB-MLI GCPVS with dynamic performance based on the proposed MPPT technique.

Table 5.1 Main designed parameters of two CHB-MLI for GCPVS

Parameters	Symbol	Value
PV panel		
MPP voltage in STC	V_{mpp}	63 V
MPP current in STC	I_{mpp}	0.92 A
PV array		
Rated current	I_{rated}	1.84 A
Rated MPP voltage	V_{rated}	504 V
Rated maximum power	P_{rated}	928 W
Power and control scheme		
DC-link capacitor	C_1, C_2	2200 µF, 400 Vdc
PWM carrier frequency	f_{sw}	3 kHz
Single-phase utility grid	V_g, f_1	220 V_{rms}, 50 Hz
Inductor	L_f	5 mH
dc link voltage controller: PI	K_p	0.1
	K_i	1
Grid current controller: PI	K_p	15
	K_i	100

5.3.1 MPPT with rapidly changing irradiance

In order to verify the effect of using the proposed MRCC-MPPT technique to control the two H-bridge cells CHB-MLI for GCPVS in the two situations of rapidly shading irradiance. In case 1, both PV strings, PV_1 and PV_2, were shaded from irradiance in the same time and power from the irradiation as shown in Figure 5.6 (a). In case 2, only the PV string of H-bridge2 PV_2 was under shading conditions and the PV_1 was operated in the constant irradiance as shown in Figure 5.9 (a). In both cases, the irradiance

changing is operated in 0.1 s period for the decreasing and increasing ramps. The irradiance change starts from 1000 W/m^2 to 500 W/m^2, waits at this level for 0.9 s, and increases again from 500 W/m^2 to 1000 W/m^2, with a constant slope. The temperature is considered 35°c during the simulation.

Figure 5.6 and Figure 5.9 show the simulation results of the proposed control method in case 1 and case 2 of irradiance profiles, respectively. From the features of the PV system, the maximum total PV power generated by PV_1 and PV_2 p_{PVt} is 900W in case of without shading, 420W in case 1 and 660 W in case 2 while they are shaded.

Figure 5.6(b) and Figure 5.9(b) show the behaviors of the following variables in the condition of case 1 and case 2 respectively: the summing of both instantaneous PV powers p_{PVt}, the summing of mean input power of two H-bridge inverters p_{INVt}, the active power to grid P_{g1}, the instantaneous PV power of each PV string p_{PV1}, p_{PV2}, the mean input power of H-bridge1 and H-bridge2 inverters p_{INV1}, p_{INV2}, the mean power of capacitors p_{C1}, p_{C2}. All occurred mean values is based on the moving average function with the 10 ms of window period. The power transferred to utility grid P_{g1} came from the summing of the input power of both H-bridge inverters, multiplied to the function of CHB-MLI and subtracted the power of inductor p_L. From the results, the PV system produces the maximum power for 900W, 420W and 2000W in case of without shading, partial irradiation shading in case 2 and all irradiation shading in case 1, respectively. Although, during the PV_1 and PV_2 could not receive the same value of power as case 2, the CHB-MLI and the proposed active and reactive power controller continuously injected the maximum power to the utility grid.

Figure 5.7(a) and Figure 5.10(a) show the behaviors of the following variables in the condition of case 1 and case 2 shading respectively: the instantaneous PV voltage of each PV string v_{PV1}, v_{PV2} and PV current of each PV string i_{PV1}, i_{PV2}. In case 1 shading conditions, the behaviors of PV

voltages and PV currents supplied to both H-bridges are the same, the PV voltages v_{PV1}, v_{PV2} are changed lightly and the PV currents i_{PV1}, i_{PV2} are decreased and increased explicitly following the profile of irradiation. In case 2 shading condition, only PV current supplied to H-bridge2 i_{PV2} is decreased and increased follow the received irradiation, the PV voltage v_{PV2} is changed a little to keep the MPP of PV_2 string. From the results, the power from PV_1 and PV_2 can be controlled separately to transfer the maximum power from each PV string to the utility grid.

Figure.5.8 (a) and Figure 5.11 (a) show the waveforms of output voltage of CHB-MLI, grid current i_g, and grid voltage v_g in the case 1 and case 2, respectively. The proposed control method can control the CHB-MLI to generate the five voltage levels with sinusoidal patterns and inject the sinusoidal current which in-phase to grid voltage continuously for providing unity power factor.

Figure 5.12 (a) shows the relationship curve between PV_1 power p_{PV1} versus PV_1 voltage v_{PV1} in case 1. The curves started from the minimum PV power point at the point A and track to the MPP at the point B following the line of *p-v* characteristic curve of the irradiance 1000 W/m^2. The value of PV_1 power can be controlled to run around the MPP ($p_{PV1} = 450\text{W}$), until the irradiance profile is reduced to 500W/m^2. It causes the value of PV_1 power p_{PV1} to be decreased to operate around the new MPP ($p_{PV1} = 200\text{W}$), at point C. The irradiance profile is waited in this level 0.9 s and move back to the last level (1000W/m^2) again. The value of PV_1 power p_{PV1} is increased and run around MPP at the point B ($p_{PV1} = 450\text{W}$) immediately. The MPP of the PV system can be tracked immediately by the proposed MPPT method. Ann also, Figure 5.17 (b) shows the relationship curve between PV_2 power p_{PV2} versus PV_2 voltage v_{PV2} in case 1 which acts closely as the PV curve between of H-bridge1.

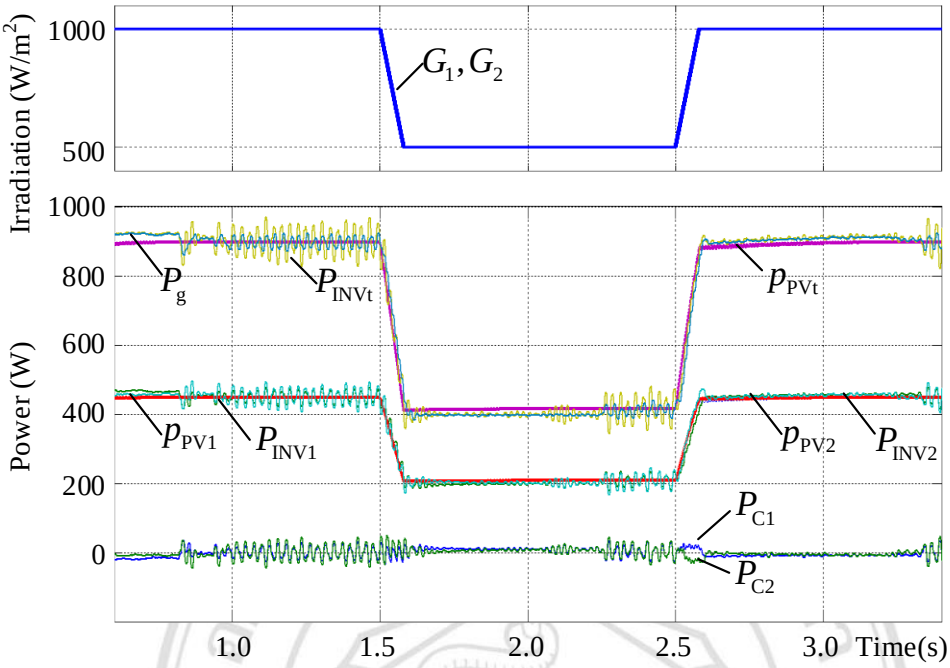

Figure 5.6 The waveform of the powers occurred in PV system during a ***case 1*** irradiance profile, using the proposed MPPT method and PQ control scheme.

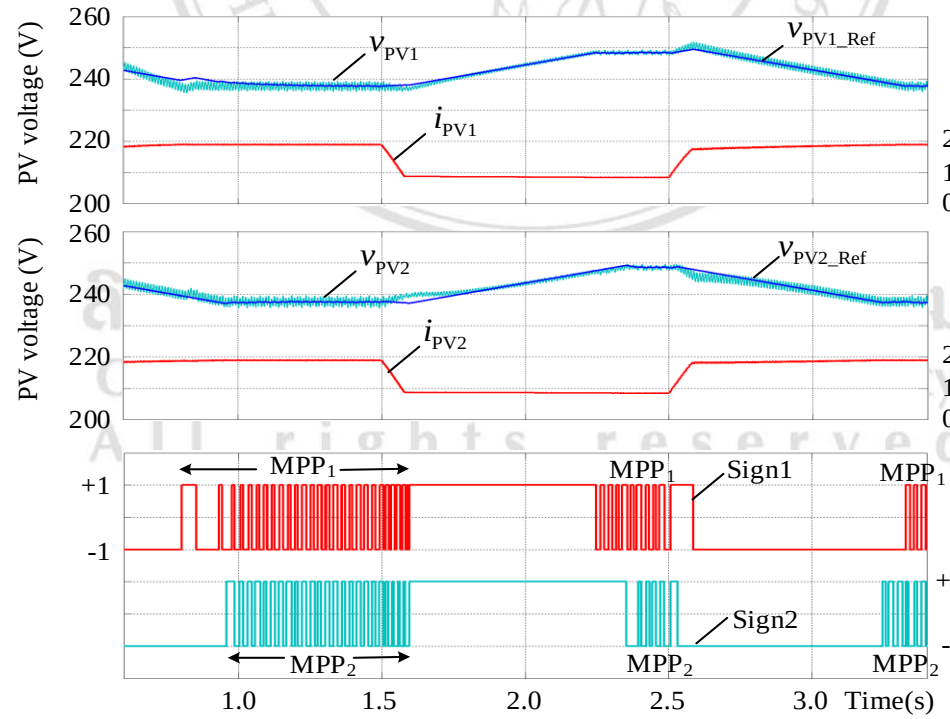

Figure 5.7 The waveform of voltages, currents in dc side, and the sign signals from the MRCC-MPPT algorithm of PV system during a ***case 1*** irradiance profile.

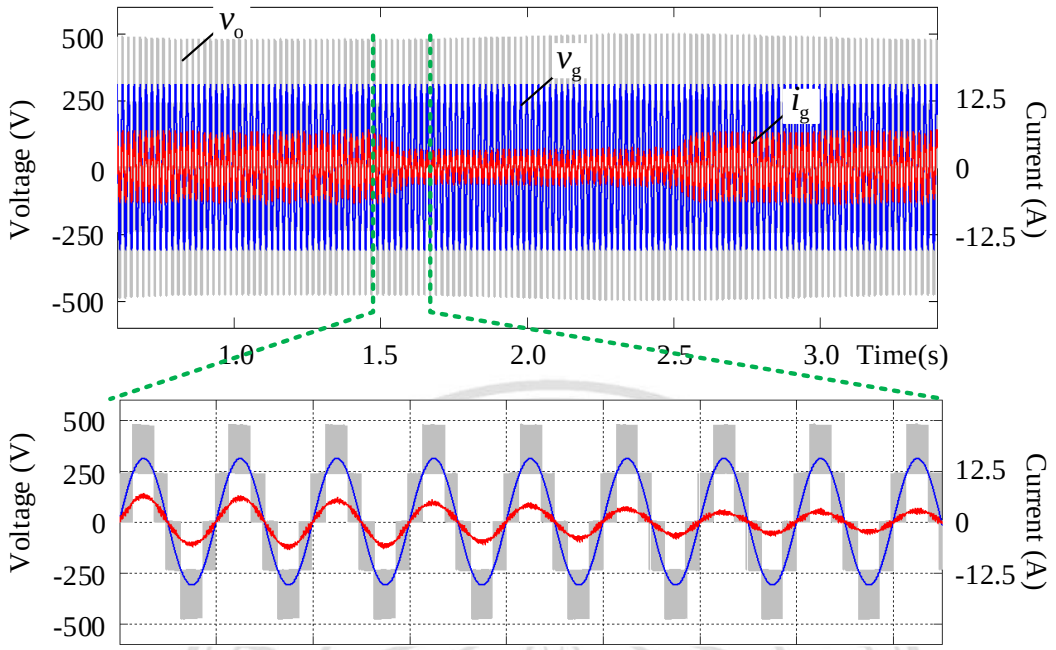

Figure 5.8 The waveform of PV system in the ac side during a ***case 1*** irradiance profile.

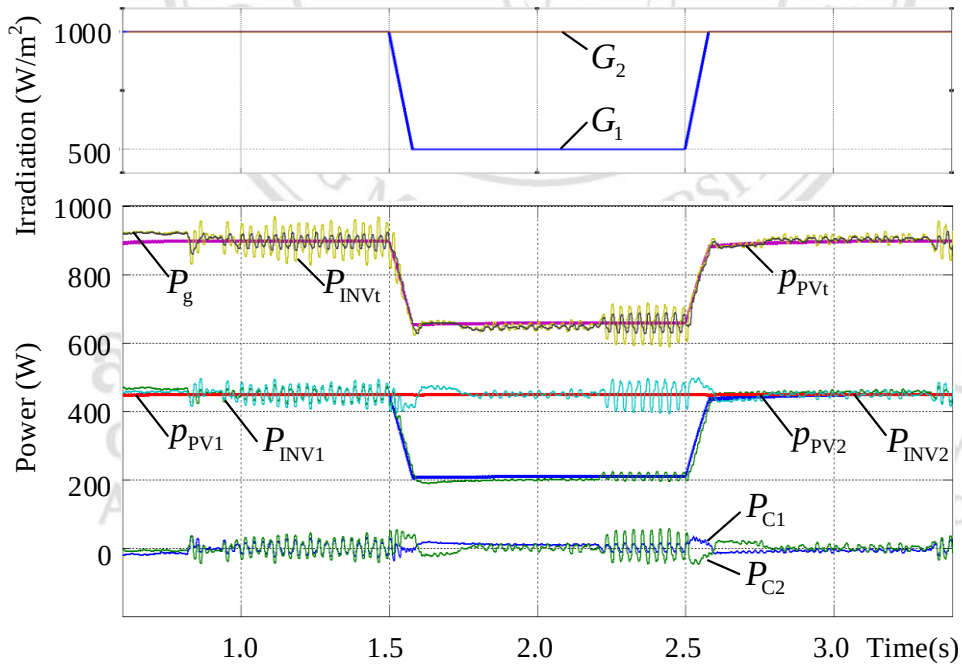

Figure 5.9 The waveform of the powers occurred in PV system during a ***case 2*** irradiance profile, using the proposed MPPT method and PQ control scheme.

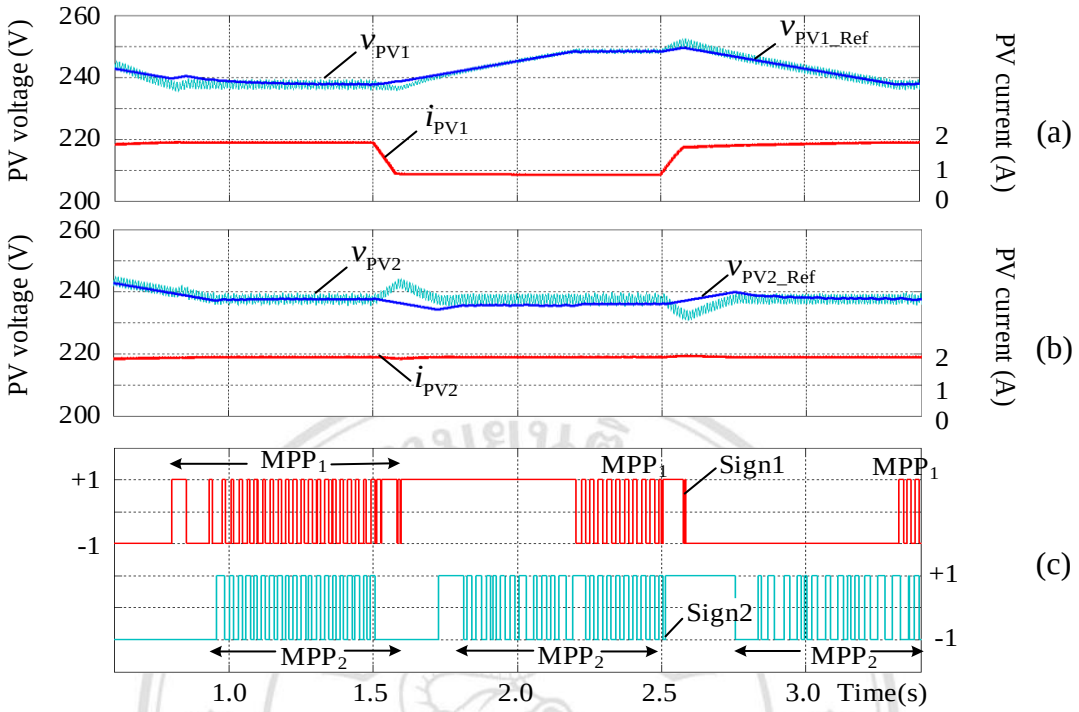

Figure 5.10 The waveform of voltages, currents in dc side, and both sign signals from both MRCC-MPPT controller of GCPVS during a ***case 2*** irradiance profile.

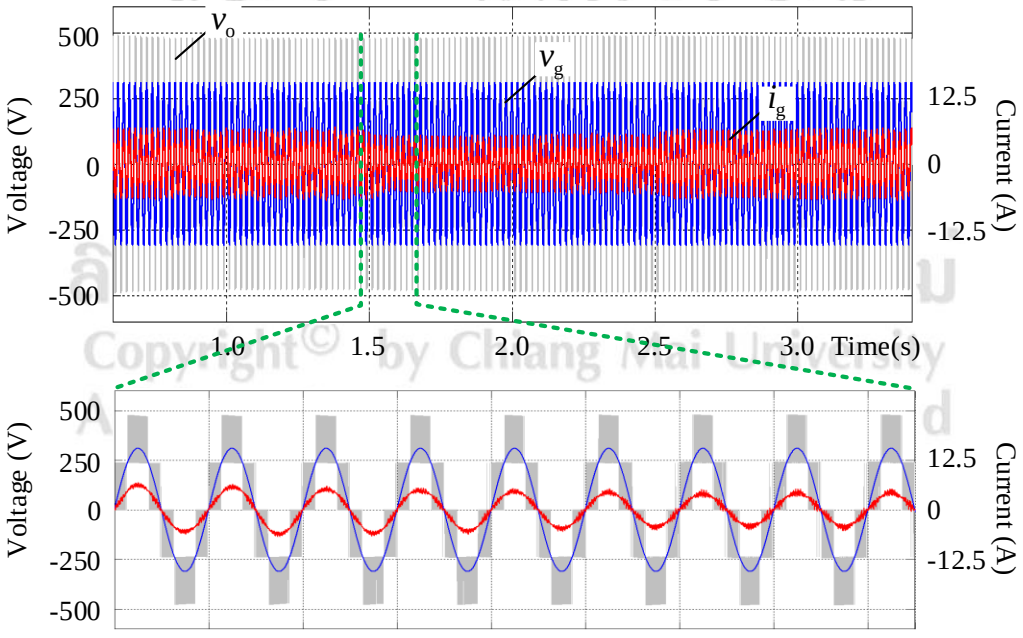

Figure 5.11 The waveform of the GCPVS in the ac side during a ***case 2*** irradiance profile.

Figure 5.13 (a) shows the relationship curve between PV_1 power p_{PV1} versus PV_1 voltage v_{PV1} in case 2. The curve is acted the same as the PV curve happened in case 1 as shown in Figure 5.10 (a). But the relationship curve between PV_2 power p_{PV2} versus PV_2 voltage v_{PV2} in case 2 is different from the act as case 1, the MPP of H-bridge2 is not changed because the irradiation of PV array2 is not changed as shown in Figure 5.10 (b). It is confirmed that each H-bridge can track its MPP independently and accurately.

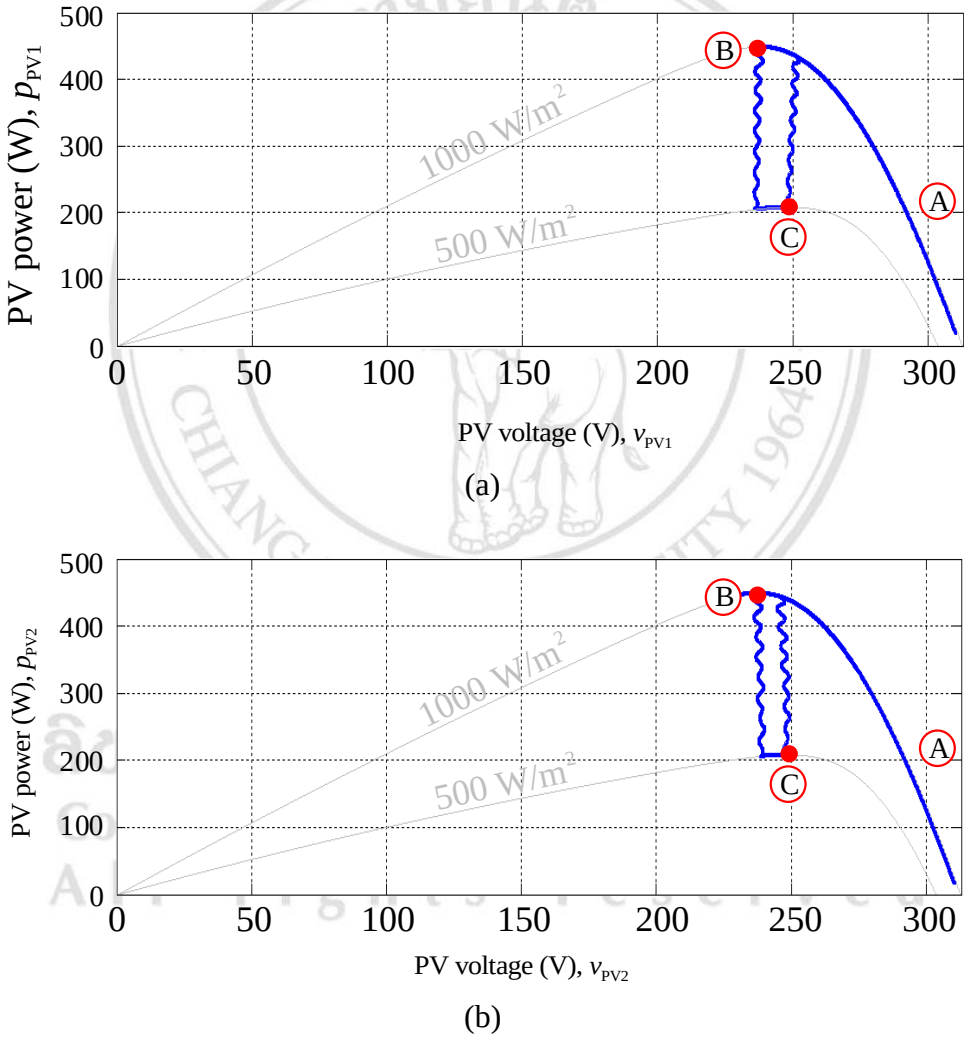

Figure 5.12 The relationship curve between PV power versus PV voltage in case 1 (all PV array irradiation shading), (a) H-bridge1 p_{PV1} and v_{PV1}, (b) H-bridge2 p_{PV2} and v_{PV2}.

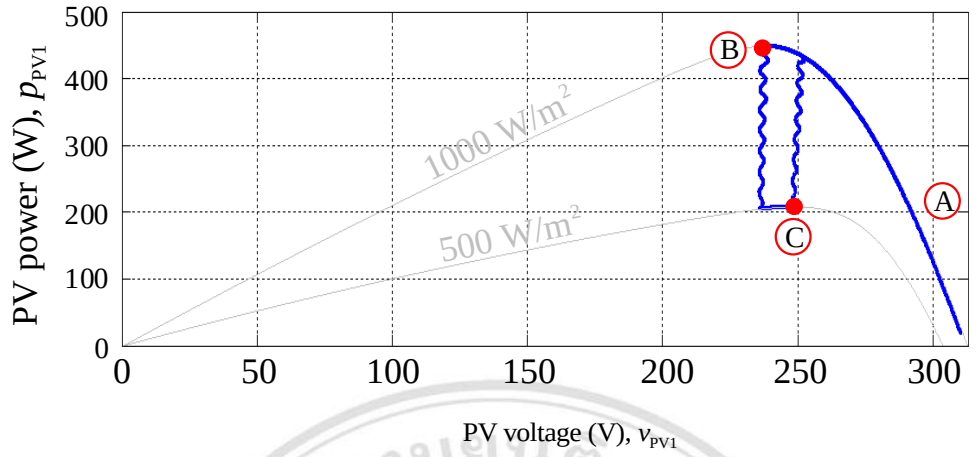

(a)

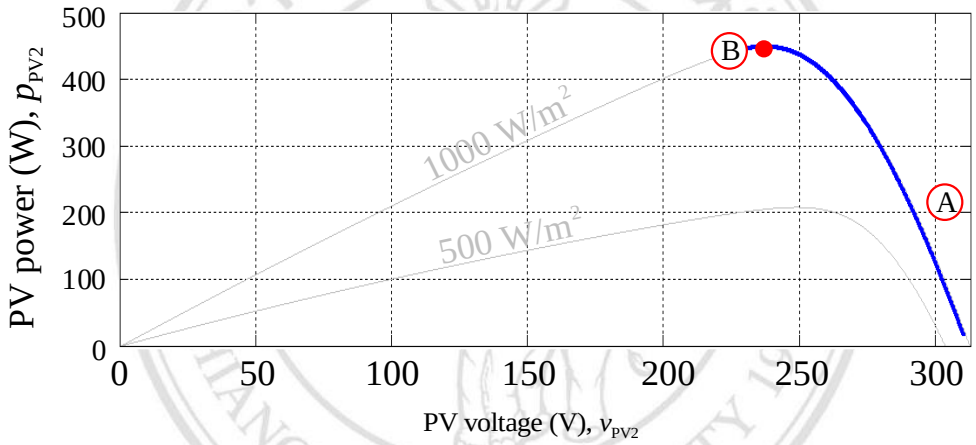

(b)

Figure 5.13 The relationship curve between PV power versus PV voltage in case 2 (partial PV array irradiation shading), (a) H-bridge1 p_{PV1} and v_{PV1},(b) H-bridge2 p_{PV2} and v_{PV2}.

5.3.2 Active and reactive power control

Figure 5.14 shows the simulation results of active and reactive power controlled with the proposed control technique, during constant irradiation. In Figure 5.14(a), the grid current i_{gd}, i_{gq} can be controlled by adjusting the grid current references of the active current i_{gd}^* and the reactive current i_{gq}^*. The dynamic response of the CHB-MLI is simulated to three steps changed in reactive current reference i_{gq}^*.

The step settings of reactive current reference are stepped from 0A to - 2A, -2A to +2A, and +2A to 0A, respectively. They caused the injected reactive power Q_g changed from 0 to -300 var, -300 var to +300 var, and +300 var to 0, respectively, which corresponded to reactive power Q_{g1} calculated in fundamental formulas, as shown in Figure. 5.14 (b). Although, the reactive power of the system are changed in three steps as the mentions, The PV power p_{PV} is still extracted and operated around the MPP continuously through the period of testify as confirmed the sign signals from the proposed MRCC-MPPT control block of the both H-bridges, as shown in Figure 5.14(c).

In Figure 5.14 (d), it can be seen that the phase current of CHB-MLI can operate under the in-phase, lagging and leading power factor conditions with the phase-angles ϕ_1 are $0°$, $-19.2°$, $+19.2°$, and $0°$, respectively. The injected active power P_g is almost constant at 900 W (P_{MPP}). However, there was some slightly changed of active power P_g while the reactive current reference i_{gq}^* is stepped. The output voltage of CHB-MLI v_o can be generated in five voltage levels with high output frequency $f_o = 12$ kHz while the PWM carrier frequency $f_{cr} = 3$ kHz, The total harmonic distortion (THD) of grid current i_g and the output voltage of CHB-MLI v_o are 4.21% and 42.88%, respectively.

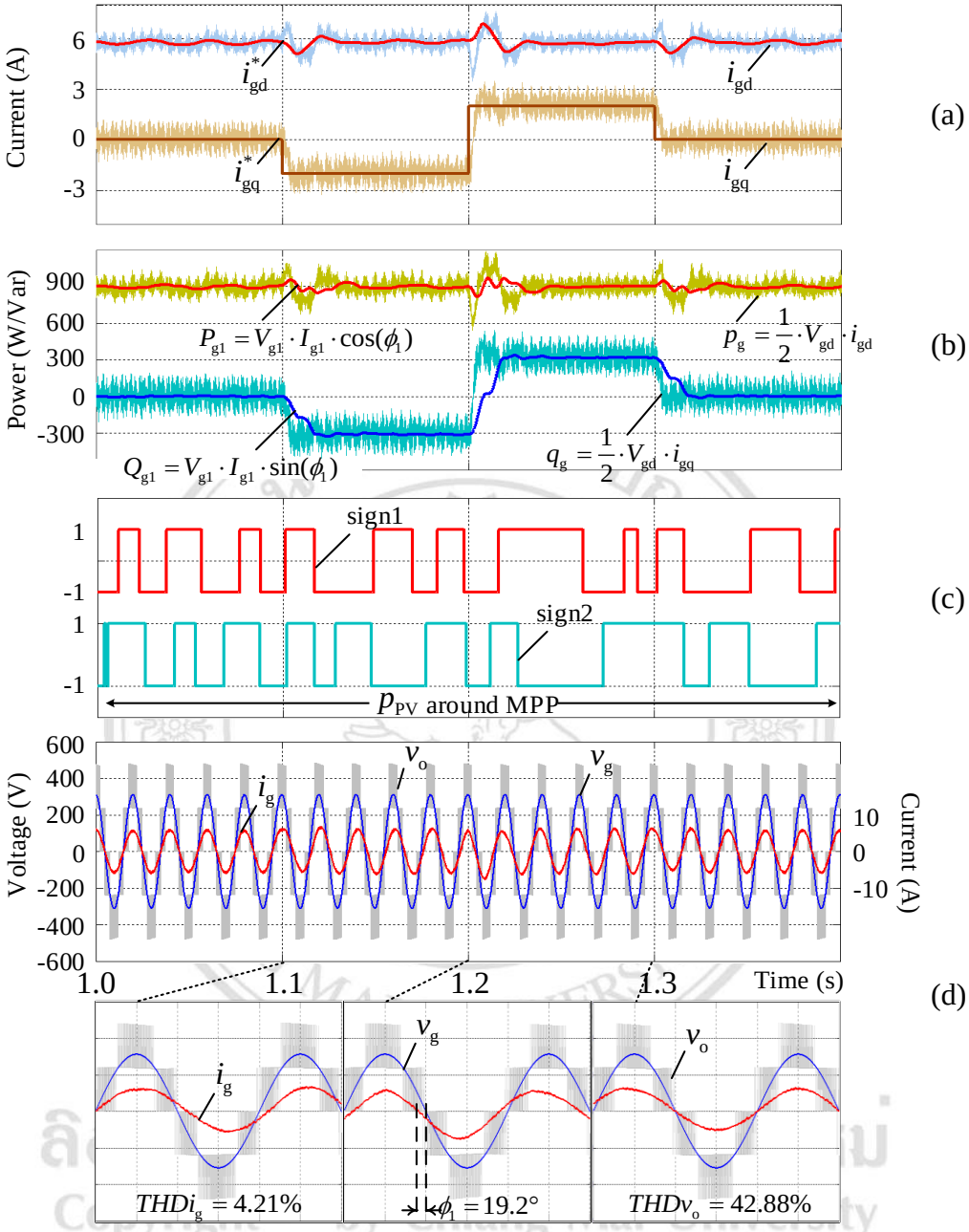

Figure 5.14 Results of the active and reactive power control (a) Reference Grid currents i^*_{gd}, i^*_{gq} and grid currents i_{gd}, i_{gq}, (b) active power p_g and reactive power q_g,and the fundamental active power P_{g1} and reactive power Q_{g1}, (c) the sign signals of upper and lower H-bridge cells, sign1and sign2 .(d) the waveform of output voltage v_o, grid voltage v_g and grid current i_g with three periods extended.

5.4 Experimental results

In this section, the proposed system presented by the single-stage single-phase CHB-MLI GCPVS and the modified RCC-MPPT method, as shown in Figure 5.2, has been verified by the simulation using the MATLAB/Simulink environment according the last topic and the experimental implementation has been carried out on the laboratory prototype. It consists of two major parts. Part one is the controller using a dSPACE DS1104 controller via a CLP1104 Input/Output interface boards commanded by the programmable computer (PC) system, where the sampling time rates of the cascade loop control given by the dc voltage control and the grid connected current control are set at 1000 μs and 100 μs, respectively. The second part is the hardware included in the PV array source and the grid-connected VSI, which is controlled by the PWM signals with a deadtime of 4 μs. For a direct comparison, the parameters are set to be the same for both the simulation and experiment, as shown in Table 5.1. Significantly, the investigation is designed to regard the following points: 1) to demonstrate and analysis of the PS-CBPWM technique for two cascaded H-bridges multilevel VSI. 2) to demonstrate the grid current control based on the *dq* vector control. 3) to demonstrate the dynamic performance of the proposed modified RCC-MPPT algorithm applied in the single-stage single-phase CHB-MLI GCPVS for interfacing with the single-phase utility grid and to evaluate the efficiency of the proposed system.

5.4.1 Analysis of the PS-CBPWM technique for two cascade H-bridge multilevel VSI

In this section, to analysis and verify by using the PS-CBPWM technique for two cascade H-bridges multilevel VSI with simulation and experimental results of this technique are presented. The modeling of the two single-phase cascade H-bridge inverters, using the PS-CBPWM strategy, was implemented in Matlab/Simulink. The experimental setup of the proposed system is shown in Figure 5.15. It consists of two parts: a dSPACE DS1104 controller board with TMS320F240 slave processor and I/O interface board CP1104. A prototype of two H-bridge inverter modules was built in the laboratory. The specification of PV array in this experimental was 195 V_{mpp}, which comes from 3 series connections of a-Si PV module with 63 V_{mpp} and

58Wp. The setup parameters were the same as those used for the simulation. The inverter output was connected to a R-L load (625 Ω-100 mH), a non unity power factor load. The switching frequency was 750 Hz.

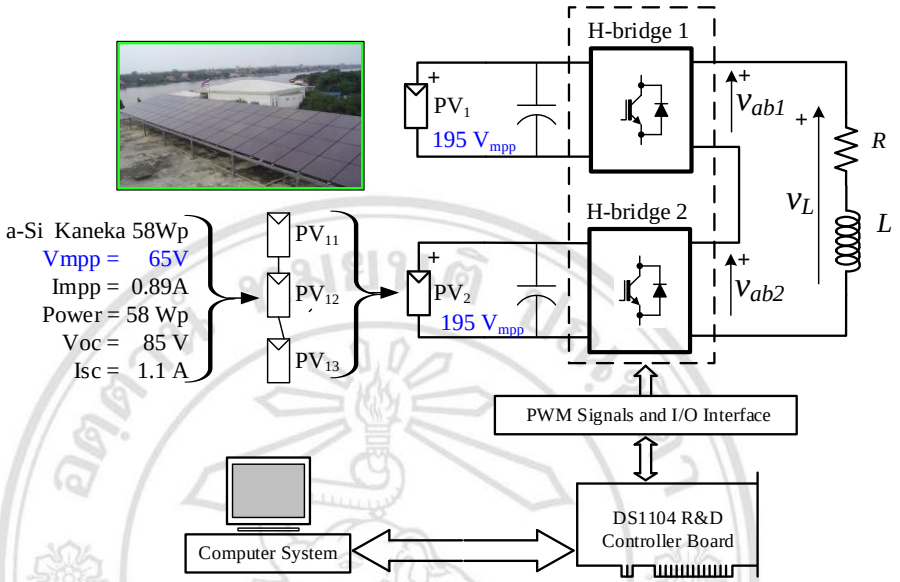

Figurer 5.15 Experimental set up.

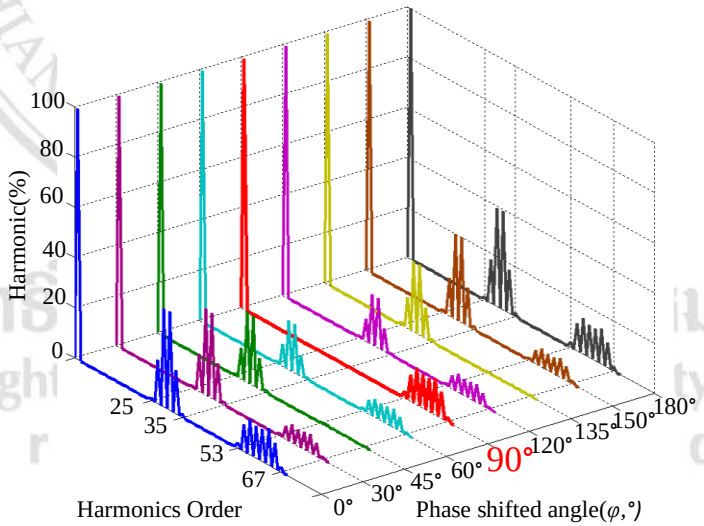

Figure 5.16 Harmonic of output voltage v_o for the 9 difference phase shifted angles φ of H_2 in condition of $m_a = 0.8$.

Figure 5.16 shows the simulation result of harmonic of output voltage v_o through fast Fourier transform (FFT) for the 9 different phase shifted angles φ of H_2 carrier signal in the condition of modulation index $m_a = 0.8$, $f_1 = 50$Hz, and $m_f = 15$. It can be seen that at the $90°$ phase shifted angle φ of H_2 carrier can produce the lowest harmonic output voltage v_o of the purposed technique, especially between harmonic order 25^{th} and 35^{th}. Figure 5.17 shows the simulation and experimental result of the THD of output voltage versus the phase shifted angle for four different values of modulation index m_a : 0.5, 0.8, 1.0 and 1.2. The nine values of phase shifted angle φ of H_2, for each m_a value were selected to operate and compare between the simulation and experimental results. The result was verified that the optimization phase shifted angle φ of H_2 for two single-phase cascade H-bridge inverters when the PS-CBPWM technique is 90º. From the results, the THD of output voltage v_O of every selected value of the modulation index m_a from the experimental tests are close to the simulation results.

Figure 5.18 shows the simulation and experimental waveforms of the proposed circuit. The phase shifted angle φ of carrier waves of H_1 and H_2 are $0°$ and $90°$, respectively. The phase voltage v_{ab1}, v_{ab2}, output voltage v_o, and load phase current i_o of the inverter are shown in the condition the modulation index $m_a = 0.8$.

Figure 5.19 shows the response of output voltage v_o when $f_1 = 50$ Hz and the modulation index reference increases, starting from zero to the maximum value (0 to1.2) in 500 ms. As can be seen from simulated and measured waveforms that the output voltage has five voltage levels at high modulation index $(m_a > 0.5)$ and three voltage levels at low modulation index $(m_a \le 0.5)$.

From the results, the proposed PWM method, with 90º phase-shifted angle, allows the optimal THD of output voltage to generate five voltage levels for the solar PV standalone systems. The simulation and experimental results confirm the feasibility and reliability of the developed control scheme for two single-phase cascade H-bridge inverters with separated solar PV sources application.

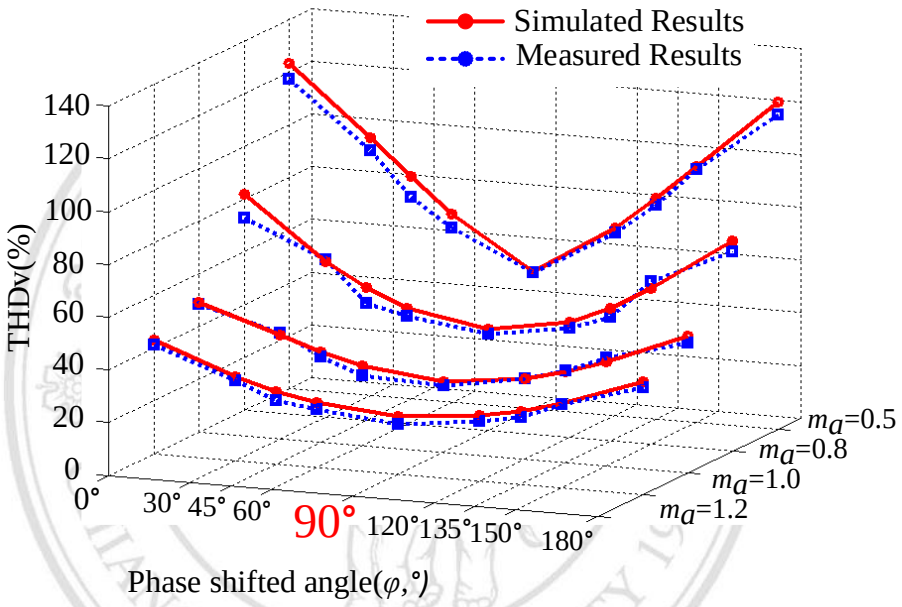

Figure 5.17 THD of output voltage v_o versus the phase shifted angle φ.

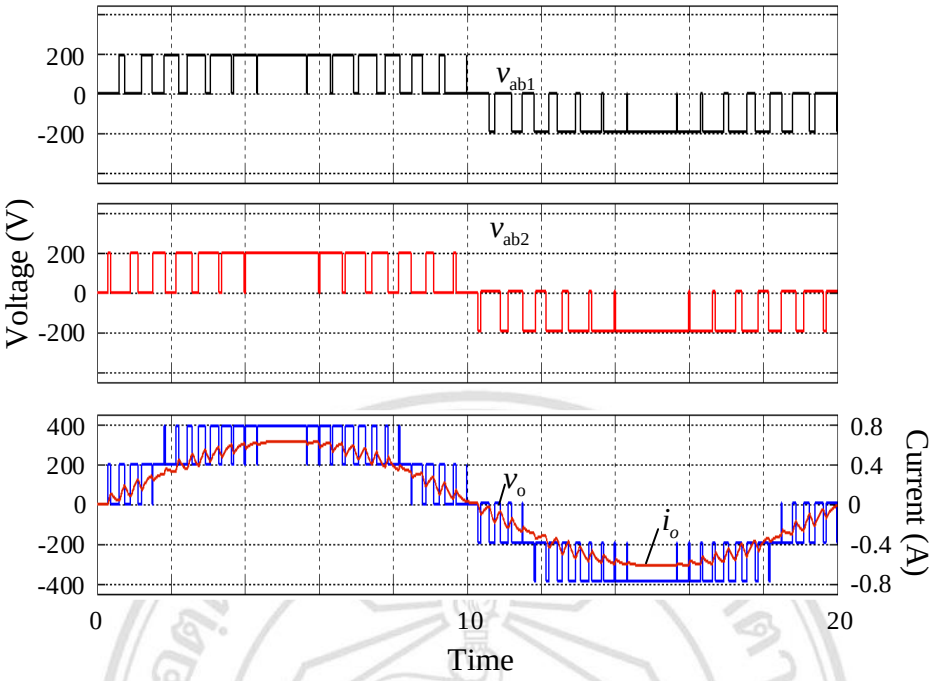

(a)

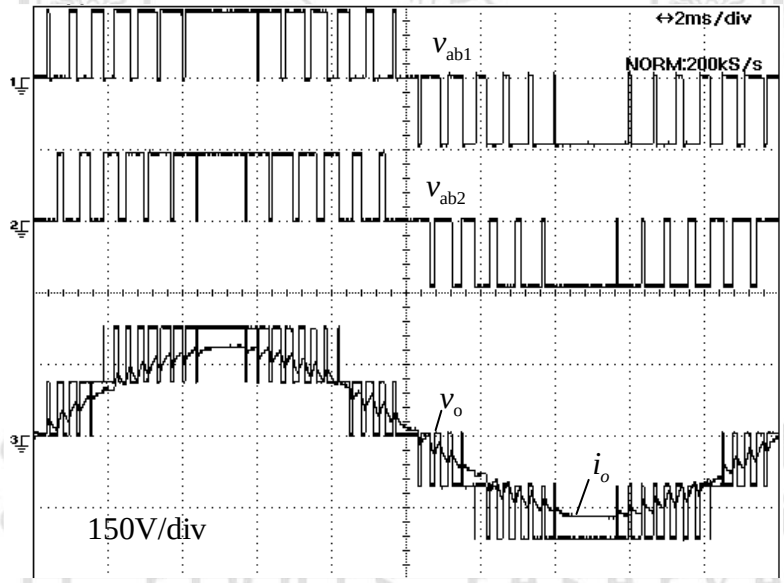

(b)

Figure 5.18 Voltage and current waveforms for $m_a = 0.8$. From inverter H_2, output voltage and load phase current for both simulation waveforms (a) and experimental waveforms (b).

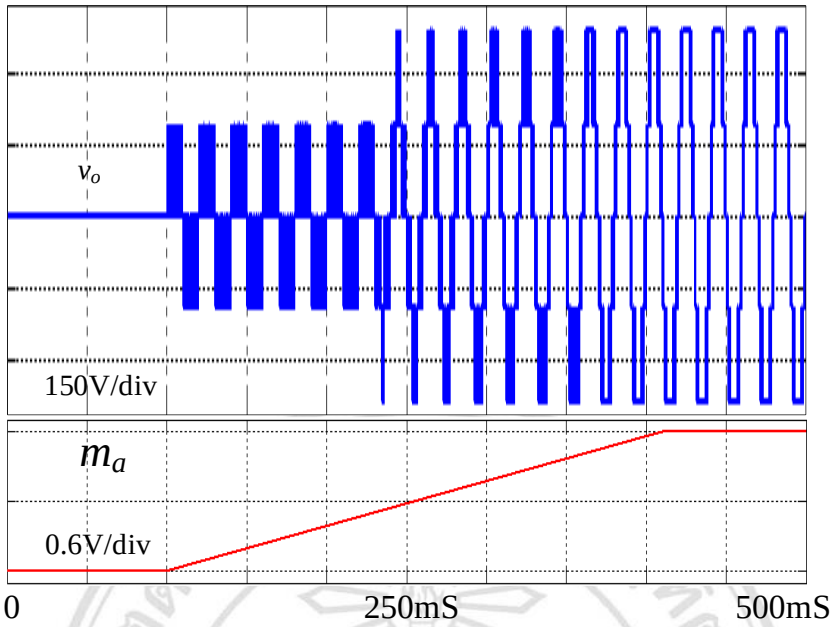

(a)

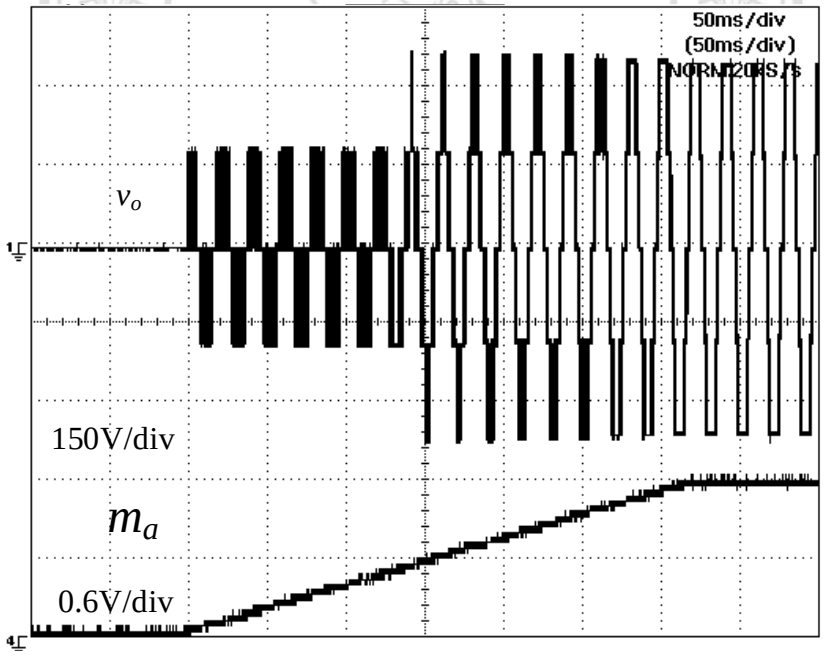

(b)

Figure 5.19 Response for a ramp input reference (a) Simulated waveforms (b) Measured waveforms.

5.4.2 The accuracy of grid current control based on the *dq* vector control

In addition to the confidence of the grid current control method based on the *dq* controller with the rotating reference frame, Figure 5.20 shows the output waveform of the CHB-MLI for grid-connected PV system while the grid current controller is operated to inject a high quality sinusoidal current i_g to the utility grid. They consisted of the output voltage of CHB-MLI v_o, the grid current i_g and the grid voltage v_g. The *dq* controller is done by commanding the peak grid current reference value $i_g^* = 3\text{A}$. The controller can generate the gate drive signals according the principle of the PS-CBPWM technique to control the two cells of CHB-MLI in order to establish perfectly sinusoidal current injected to the utility grid. From the result, it can be seen that the *dq* controller can control the grid current to act as sinusoidal with the peak current value is 3A as its command.

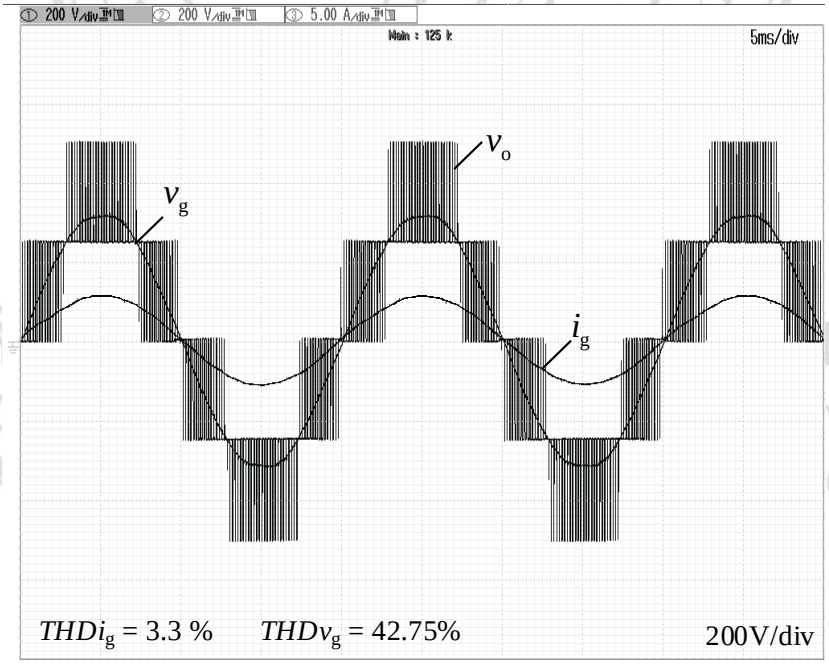

Figure 5.20 The ac side output waveforms of the single-phase single-stage CHB-MLI for GCPVS during the PV power is injected to the utility grid with unity PF.

Figure 5.21 shows the waveform of the variables in the dc and ac sides of the 928Wp single-phase single-stage CHB-MLI for GCPVS controlled with the proposed modified RCC-MPPT and the *dq* grid current controller through the prototype GCPVS in 5s period. The ac side variables consist of the output voltage of CHB-MLI v_o, the grid current i_g and the grid voltage v_g. The dc side variables are the PV power p_{PV1}, PV voltage v_{PV1} and the PV current i_{PV1} of the upper H-bridge cell. The all waveforms are started with only grid current control commanded with $i_g^* = 0\text{A}$ without the MPPT controller about 0.5s. The most of all variables are zero except the PV voltage v_{PV1} is maximum value as the open circuit PV voltage, and the output voltage of CHB-MLI v_o.controlled by grid current controller to keep $i_g = 0\text{A}$. After that the modified RCC-MPPT controller is started to control the PV system, the PV power from all 16 PV panels is extracted and injected to the grid in this period (2.5s). In this period, the PV power is injected to the grid continuously as a steady state operating. And then, the last period, the PV power is rapidly reduced 50% by disconnecting the 8 PV panels from the power circuit, providing each H-bridge cell has only 4 PV panels power source from this point through the end of this testify. From the result, the grid current controller can completely control to generate the five voltage levels and the sinusoidal current injected to the grid in both the transient and steady state operating for the CHB-MLI for GCPVS.

Figure 5.22 and 5.23 show the extended waveforms in two periods, during the startup and rapidly changing of PV power, respectively, occurred in Figure 5.21. They can be confirmed that the high performance operating of grid current controller in the dynamic operation as power startup and the very fast decreasing of PV power can be achieved completely. The CHB-MLI generates the five voltage-level to maintain the sinusoidal grid current injected to the grid continuously cover the both steady state and dynamic happens of GCPVS.

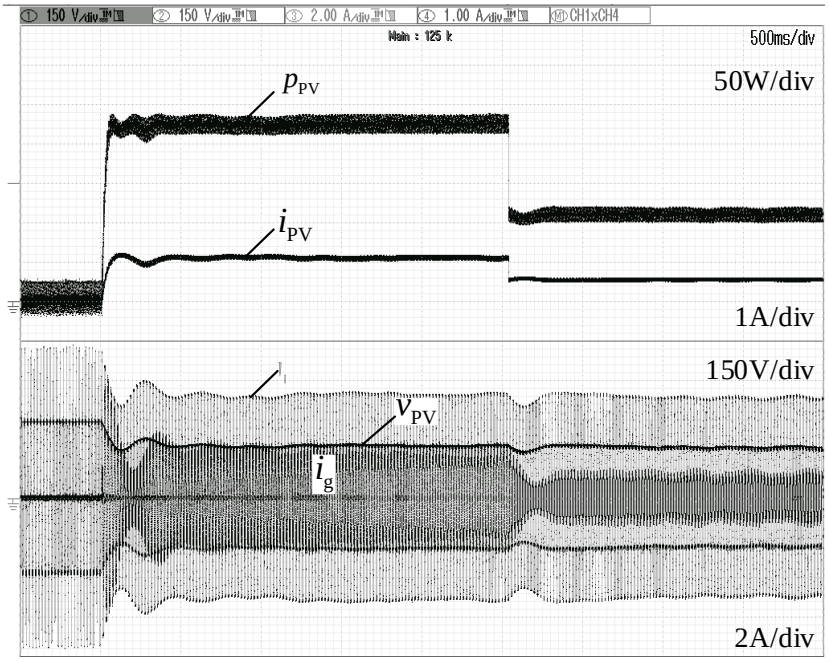

Figure 5.21 The dc and ac side waveforms of the single-phase single-stage CHB-MLI for GCPVS during the PV power is injected to the utility grid with unity PF.

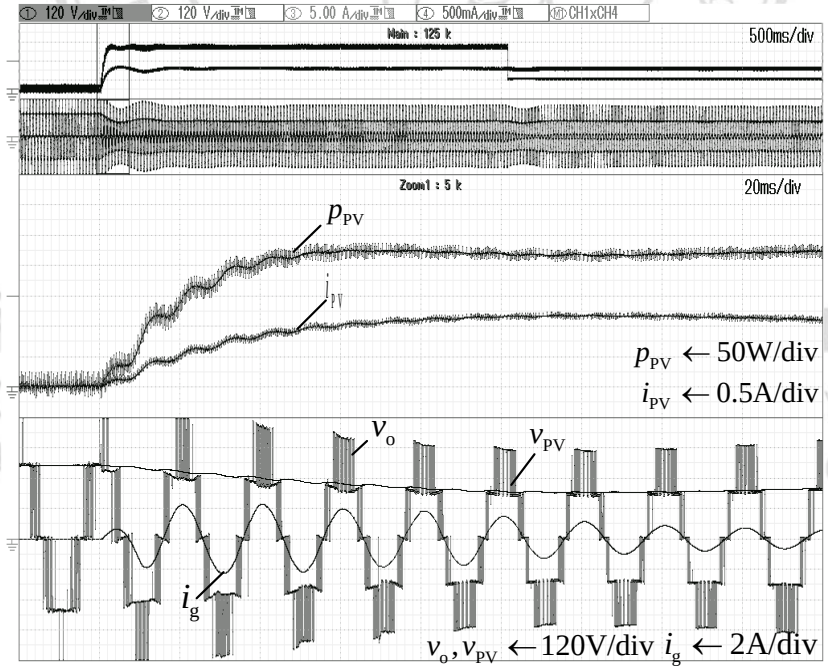

Figure 5.22 The extended waveforms of the variables during starting up from $i_g = 0$ to steady-state of the single-phase single-stage CHB-MLI for GCPVS with unity PF.

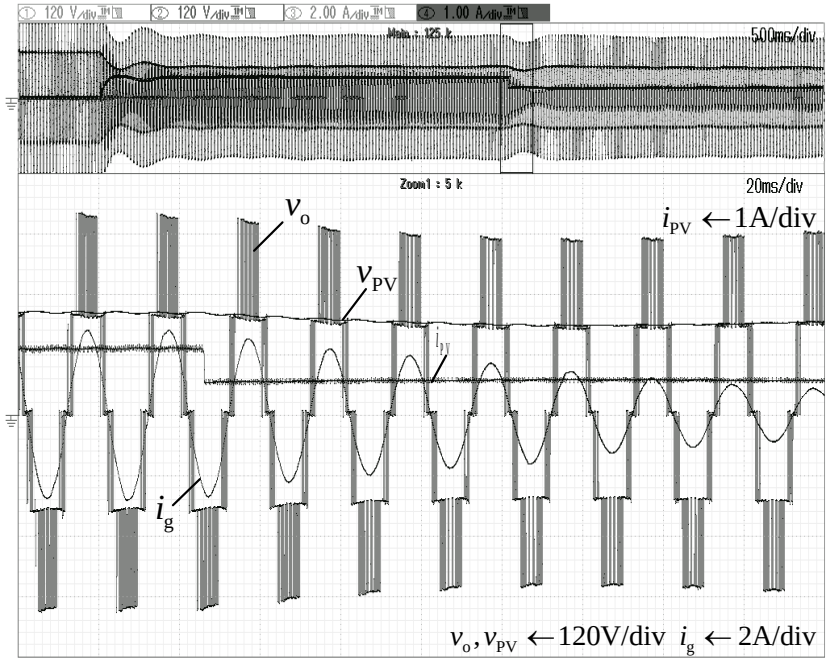

Figure 5.23 The extended waveforms of the variables during 50% rapidly PV current reduced of the single-phase single-stage CHB-MLI for GCPVS with unity PF.

5.4.3 Dynamic performance of the proposed modified RCC-MPPT algorithm applied in the single-phase single-stage CHB-MLI for GCPVS.

The step response of the system based on the proposed modified RCC-MPPT method applied in the single-phase CHB-MLI GCPVS is shown in Figure 5.24. At period A, the PV power is initially zero $p_{PV} = 0$ with the zero grid current control $i_g = 0$. The modified RCC-MPPT of both H-bridge cells are started at the end of period A, The MPP is met immediately after the MRCC-MPPT algorithm are started, it is around 300 W depended on the irradiation and ambient temperature in that time. The MPP is proofed with the PV curve as shown in Figure 5.24 (b), in period B, the PV power is operated around MPP. The very fast 50% decreasing of PV power is occurred when the 8 PV panels is disconnected immediately in period C as the aforementioned experimental and connected it back to operate in the same power-level as the last period again. Although the slop of the PV changing is very high speed as the transient, observed in Figure 5.23 (a), the system with the proposed MPPT method can immediately track the MPP.

This can also be inspected with the corresponding *P-V* curve at period B and C. In addition, The PV voltage is always run the same voltage level in both period B and C because the change of PV power is not made from the change in the irradiation or temperature providing the PV voltage is lightly changed. The experimental results are demonstrated in good agreement with corresponding behavior, as shown in Figure 5.24 (b).

In another case of the performance testify, It can be presented in Figure 5.25. The testify is started with the same act as the mention experiment in period A. The MRCC-MPPT controller is started while the PV power is 50% of all in period B. In period C, the PV power is stepped up immediately to 100% PV power in that atmospheric. After that, the PV profile is come down in two steps like a stair function. From the results, the PV system with the current control and the proposed MPPT method can immediately track the MPP in every step change. It can be confirmed that the proposed MRCC-MPPT including the *dq* current controller can track the MPP and inject that PV power to the grid with the high performance and quality.

5.5 Conclusion

This study has presented a control technique of CHB-MLI for GCPVS. The MRCC-MPPT method by using the mean function to be the main process of the maximum power transferring is proposed in order to correct the MPP operating of PV string continuously and quickly reaching MPP in case of the rapidly shading irradiation. The current control technique based-on the theoretical rotating reference frame to control the injecting of active power and reactive power independently, is proposed. From the results, they can be guaranteed that the proposed algorithm cause high accuracy and fast respond for correction the MPP in case of rapidly shading irradiance and it do not need the harmonic filter in the dc-link voltage controller. The proposed method can generate the sinusoidal grid current with low THD of grid current. Simulation and experimental results confirm the correction and reliability the developed control scheme and algorithm method with two situations, all and half PV string shading.

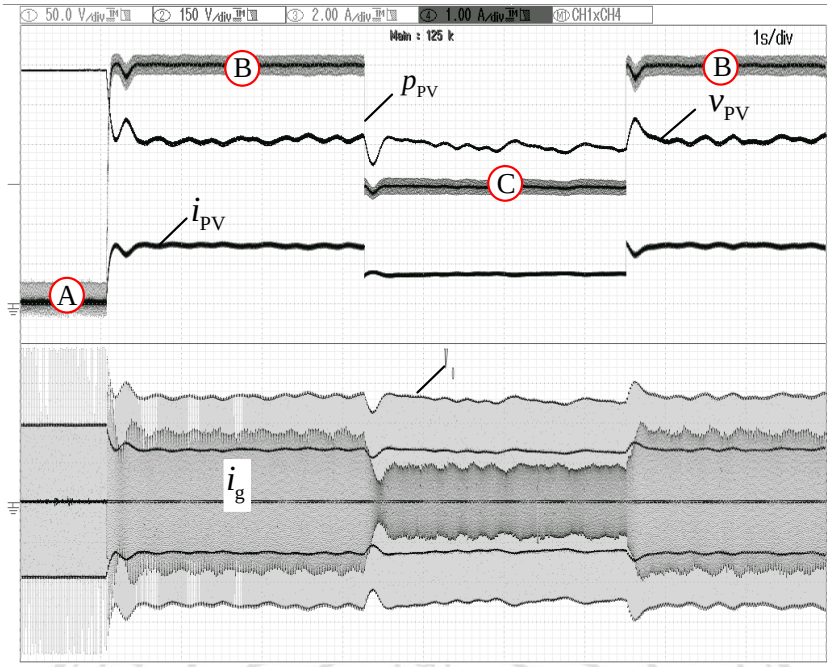

(a)

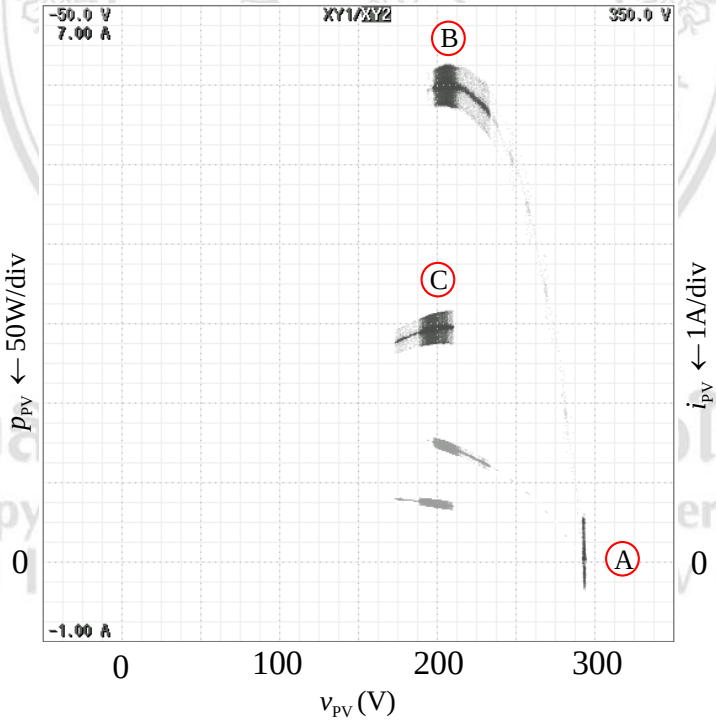

(b)

Figure 5.24 The waveforms of the variables during 50% rapidly PV power decreased and increased in the same atmospheric of the CHB-MLI for GCPVS with unity PF.

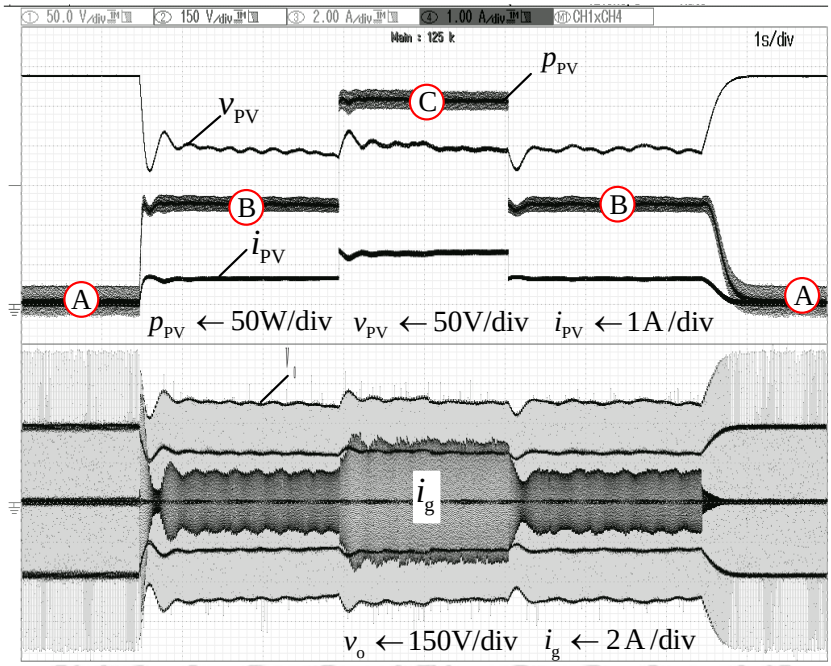

(a)

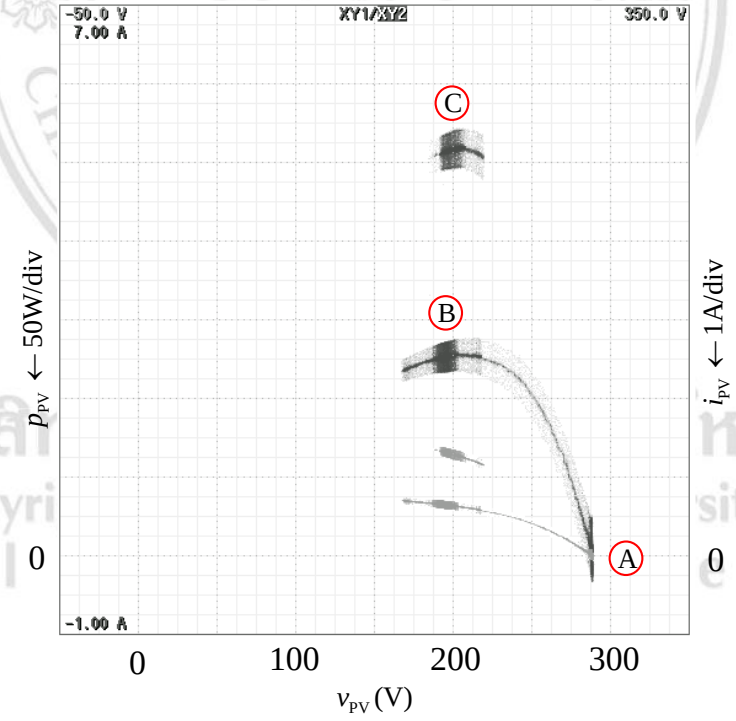

(b)

Figure 5.25 The waveforms of the variables during 50% rapidly PV power increased and decreased in the same atmospheric of the CHB-MLI for GCPVS with unity PF.